



Joint interpretation of enantiomer and stable isotope fractionation for chiral pesticides degradation

Jin, Biao; Rolle, Massimo

Published in:
Water Research

Link to article, DOI:
[10.1016/j.watres.2016.08.057](https://doi.org/10.1016/j.watres.2016.08.057)

Publication date:
2016

Document Version
Peer reviewed version

[Link back to DTU Orbit](#)

Citation (APA):

Jin, B., & Rolle, M. (2016). Joint interpretation of enantiomer and stable isotope fractionation for chiral pesticides degradation. *Water Research*, 105, 178-186. DOI: [10.1016/j.watres.2016.08.057](https://doi.org/10.1016/j.watres.2016.08.057)

DTU Library

Technical Information Center of Denmark

General rights

Copyright and moral rights for the publications made accessible in the public portal are retained by the authors and/or other copyright owners and it is a condition of accessing publications that users recognise and abide by the legal requirements associated with these rights.

- Users may download and print one copy of any publication from the public portal for the purpose of private study or research.
- You may not further distribute the material or use it for any profit-making activity or commercial gain
- You may freely distribute the URL identifying the publication in the public portal

If you believe that this document breaches copyright please contact us providing details, and we will remove access to the work immediately and investigate your claim.

This is a Post Print of the article published on line 30th August 2016 in Water Research, 105, 178-186. The publishers' version is available at the permanent link:

<http://dx.doi.org/10.1016/j.watres.2016.08.057>

Joint interpretation of enantiomer and stable isotope fractionation for chiral pesticides degradation

Biao Jin^a and Massimo Rolle^{a,*}

^a Department of Environmental Engineering, Technical University of Denmark, Miljøvej Building
113, DK-2800 Kgs. Lyngby, Denmark

* Corresponding author phone: +45 45251566; e-mail: masro@env.dtu.dk

Highlights

- Integrated model for concentrations, enantiomers and stable isotopes fractionation
- Joint quantitative approach to interpret dual enantiomer and stable isotope data
- Characterization of isotope and enantiomer selective reaction mechanisms
- Model validation based on chiral pesticides degradation data

1 **Abstract**

2 Chiral pesticides are important contaminants affecting the health and functioning of aquatic systems.
3 The combination of stable isotope and enantiomer analysis techniques has been recently proposed
4 to better characterize the fate of these contaminants in natural and engineered settings. We
5 introduce a modeling approach with the aim of unifying and integrating the interpretation of
6 isotopic and enantiomeric fractionation. The model is based on the definition of enantiomer-specific
7 isotopologues and jointly predicts the evolution of concentration, enantiomer fractionation, as well
8 as changes in stable isotope ratios of different elements. The method allows evaluating different
9 transformation pathways and was applied to investigate enzymatic degradation of dichlorprop
10 (DCPP), enzymatic degradation of mecoprop methyl ester (MCPPM), and microbial degradation of
11 α -hexachlorocyclohexane (α -HCH) by different bacterial strains and under different redox
12 conditions. The model accurately reproduces the isotopic and enantiomeric data observed in
13 previous experimental studies and precisely captures the dual-dimensional trends characterizing
14 different reaction pathways. Furthermore, the model allows testing possible combinations of
15 enantiomer analysis (EA), compound specific isotope analysis (CSIA), and enantiomer specific
16 isotope analysis (ESIA) to identify and assess isotope and enantiomer selective reaction
17 mechanisms.

18

19 *Keywords:* Pesticides; Enantiomer analysis; CSIA; ESIA; Degradation pathways

20

21

22

23

24

25 **1. Introduction**

26 Organic pesticides are applied in many anthropogenic activities and constitute an increasing threat
27 to the quality and health of aquatic systems (Fenner et al., 2013; Schwarzenbach et al., 2006).
28 Pesticides are frequently detected in drinking water wells (Spliid and Køppen, 1998; Turner et al.,
29 2006; Vorkamp et al., 2014) and are a primary reason causing the shutdown of drinking water
30 supplies (e.g., Thorling, 2015). Pesticides can bypass wastewater treatment plants and enter natural
31 aquatic systems (Lapworth et al., 2012; McKnight et al., 2015; Pal et al., 2010) posing serious risks
32 to aquatic life and human health (Schwarzenbach et al., 2010). Chiral compounds represent an
33 important fraction of organic pesticides released in the environment (Wong, 2006; Zipper et al.,
34 1998). These chemicals are dispensed as mixtures of two enantiomers (i.e., a pair of molecular
35 entities which are mirror images of each other and nonsuperposable, IUPAC 2014). They are of
36 special interest and concern due to the fact that stereoisomers of one chiral compound often have
37 different biological fate and toxic effects (Bollmann et al., 2014; Petrie et al., 2014). Thus, detailed
38 understanding of the environmental distribution and the degradation processes of chiral pesticides is
39 essential for risk assessment and for evaluating the hazardous effects of these organic compounds in
40 both wastewater treatment systems and natural aquatic environments (Stenzel et al., 2013; Wong,
41 2006).

42 Due to the complexity in assessing the fate of organic pollutants in environmental systems, where
43 intricate and coupled physical and biochemical processes hinder quantitative evaluations, it is
44 necessary to combine conventional and innovative approaches. Concentration analyses of mother
45 compounds and their metabolites are typically applied and represent a primary source of
46 information. However, this approach is often not conclusive, since it is hampered by the difficulty
47 to distinguish between transformation and dilution processes. For chiral compounds, enantiomer

48 analysis (EA) is an additional valuable tool to demonstrate the occurrence of biotransformation
49 processes (Rügge et al., 2002). This approach analyzes changes of enantiomeric compositions
50 occurring during enantioselective biochemical transformations. Another independent approach is
51 compound specific isotope analysis (CSIA) which determines the isotopic evolution during
52 degradation processes. Recently, stable isotope techniques have been developed at a fast pace and
53 applied in various experimental (e.g., Sakaguchi-Söder et al., 2007, Bashir et al., 2015; Elsayed et
54 al., 2014; Jin et al., 2014; Rolle et al., 2010; Schmidt and Jochmann, 2012) and modeling studies
55 (e.g., Prommer et al., 2009; Eckert et al., 2012; Jin et al., 2013; Thullner et al., 2012; Van Breukelen
56 and Rolle, 2012). A further advance is enantiomer specific isotope analysis (ESIA), which allows
57 analyzing the isotopic composition of individual enantiomers (Badea et al., 2011; Maier et al.,
58 2013). Facilitated by the developments of analytical techniques, a number of recent experimental
59 studies have proposed to combine enantiomer and isotope analyses to investigate the fate of
60 different chiral organic pollutants, including phenoxy acids (Milosevic et al., 2013; Qiu et al., 2014),
61 hexachlorocyclohexane isomers (Badea et al., 2011; Bashir et al., 2013) and phenoxyalkanoic
62 methyl herbicides (Jammer et al., 2014). Such approach has shown great potential to decipher
63 degradation mechanisms of different chiral compounds. In fact, different reaction pathways are
64 characterized and effectively visualized by plotting enantiomer ratios together with stable isotope
65 ratios (Bashir et al., 2013; Jammer et al., 2014; Milosevic et al., 2013; Qiu et al., 2014). During the
66 reaction of chiral organic contaminants, stable isotope fractionation occurs due to mass differences
67 of isotopologues of individual enantiomers. Specifically, the mass differences of isotopologues
68 result in different bond strength, and thus undergo reaction processes at different rates. Enantiomers,
69 instead, have the same mass and bond energy, therefore enantiomer enrichment in a biochemical
70 reaction is due to different geometrical recognitions of the two enantiomer molecules (Jammer et al.,
71 2014; Wong, 2006). Although the fractionation of stable isotope and enantiomers is due to different

72 mechanisms, they are intimately related and occur simultaneously. Even though isotope and
73 enantiomer fractionation occur simultaneously during chiral pesticide degradation, the two
74 fractionating systems are evaluated independently and, only subsequently, they are merged in two-
75 dimensional representations for mechanistic interpretation. Therefore, a first-principle based
76 modeling approach aiming at unifying the information gained from enantiomer and stable isotope
77 analyses is required. Such development will contribute to improve our capability to interpret
78 combined enantiomer and isotope signals, as well as to overcome some of the challenges emerging
79 from experimental studies in which nonlinear patterns are commonly observed due to the
80 significantly different extents of enantiomer and stable isotope fractionation.

81 The objective of this work is to provide an integrated evaluation scheme to describe and interpret
82 the evolution of enantiomer and stable isotope ratios during the degradation of chiral pollutants. The
83 proposed framework allows the joint and simultaneous description of: (i) concentrations of parent
84 compounds and metabolites, (ii) enantiomer fractionation, and (iii) stable isotope evolution. The
85 approach is validated with recently published concentration, enantiomer and stable isotope data of
86 important chiral pesticides such as dichlorprop (DCPP), mecoprop methyl ester (MCPPM) and α -
87 hexachlorocyclohexane (α -HCH). The model is also used to test the applicability and the potential
88 of different two-dimensional approaches combining stable isotope fractionation (as individual
89 enantiomers or as compound average) with enantiomer analysis to characterize different reaction
90 mechanisms of chiral pesticides degradation.

91

92 **2. Material and methods**

93 **2.1. Enantiomer-specific isotope modeling**

94 The modeling framework originates from the main idea of incorporating mechanistic information
95 on contaminants degradation in model-based interpretation of stable isotope data (Jin and Rolle,

96 2014). A major challenge addressed by the proposed approach is to consistently integrate the
 97 quantitative description of enantiomer and stable isotope evolution. Enantiomers are normally
 98 denoted according to their molecular configuration (*R* and *S*) or optical activity (+ and -) (Wong,
 99 2006). To illustrate our approach, we consider an example using *R* and *S* enantiomers undergoing
 100 different extents of degradation and resulting in the enrichment of one enantiomer. An example
 101 using the optical activity notation is outlined in the last section of the Supplementary Material.
 102 Besides enantioselectivity, the cleavage of chemical bonds during degradation of a chiral compound
 103 also causes stable isotope fractionation in both *R* and *S* enantiomeric molecules. As many organic
 104 micropollutants, chiral organic pesticides often have large molecular size and thus it is efficient to
 105 track directly the atoms experiencing isotope effects during transformation processes (Jin and Rolle,
 106 2015). Therefore, it is convenient to define enantiomer-specific isotopologues: enantiomer
 107 molecules with different isotopic compositions at reactive positions. The proposed model can be
 108 formulated for single- and multi-element isotope fractionation. In the following we illustrate the
 109 procedure for a dual-element system. Considering the occurrence of isotopically-sensitive atoms of
 110 two elements, X and Y, the relative abundances of the j^{th} enantiomer-specific isotopologues for *R*
 111 and *S* enantiomers are given by the product of the abundance of each isotope (Hofstetter et al., 2007;
 112 Sakaguchi-Söder et al., 2007):

$$A_j^R = \prod_{i=1}^{m_X} (X_{H,i}^{v_i} \cdot X_{L,i}^{1-v_i}) \cdot \prod_{h=1}^{m_Y} (Y_{H,h}^{u_h} \cdot Y_{L,h}^{1-u_h}) \quad (1)$$

$$A_j^S = \prod_{i=1}^{m_X} (X_{H,i}^{v_i} \cdot X_{L,i}^{1-v_i}) \cdot \prod_{h=1}^{m_Y} (Y_{H,h}^{u_h} \cdot Y_{L,h}^{1-u_h}) \quad (2)$$

113 where A_j^S and A_j^R are the relative abundances of the j^{th} enantiomer-specific isotopologue of *R* and *S*
 114 enantiomer. A_j^S and A_j^R are expressed considering exclusively the isotope abundances of atoms X
 115 and Y at fractionating positions. Each enantiomer isotopologue can contain up to m_X , total X atoms,

116 and m_Y , total Y atoms, at fractionating positions. The indexes i and h identify X and Y atoms,
117 respectively, at different fractionating positions within a given molecule. X and Y are the
118 abundances of X and Y isotopes, respectively. Such abundances are raised to the exponents v and u ,
119 which can assume binary values (0 or 1) accounting for the occurrence of heavy (i.e., $v=1$; $u=1$) and
120 light (i.e., $v=0$; $u=0$) isotopes at each fractionating position.

121 For a specific reaction, isotopes of one element in the j^{th} enantiomer-specific isotopologue are
122 fractionating according to the corresponding apparent kinetic isotope effect, AKIE (Elsner et al.,
123 2005):

$$\alpha^R = AKIE_R^{-1} \approx 1 + \frac{n_R}{m_R} \cdot \varepsilon_{bulk}^R \quad (3)$$

$$\alpha^S = AKIE_S^{-1} \approx 1 + \frac{n_S}{m_S} \cdot \varepsilon_{bulk}^S \quad (4)$$

124 These equations can be written both for X and Y isotopes. α is the fractionation factor for the R or
125 S enantiomer, ε is the bulk enrichment factor of individual enantiomers, n is the total number of
126 atoms of X or Y element in one enantiomer molecule, m is the number of atoms of one element
127 located at fractionating positions in the R or S enantiomer. Accurate estimates of AKIE values are
128 important for the proposed modeling approach. Besides the calculations based on Eqs. 3 and 4, the
129 advances in analytical techniques, as well as in theoretical calculations and computational chemistry,
130 are likely to provide more direct insight on AKIEs based on position-specific isotope measurements,
131 as well as on computational chemistry predictions (e.g., Breider and Hunkeler, 2011; Grzybkowska
132 et al., 2014; Świderek and Paneth, 2012; Wuerfel et al., 2013).

133

134 We track the concentration evolution of each enantiomer-specific isotopologue according to a
135 specified kinetic rate law. To demonstrate the approach we consider a first-order kinetic, however

136 the model is quite general and similar governing equations can be formulated for more complex
 137 degradation kinetics, including Michaelis-Menten kinetic coupling the contaminant degradation to
 138 biomass dynamics (see details in the Supplementary Material). For a first-order reaction rate, the j^{th}
 139 enantiomer-specific isotopologues of R and S enantiomers can be defined as:

$$r_j^R = k_R \cdot C_j^R \cdot \prod_{i=1}^{m_X} (\alpha_{X,i}^R)^{v_i} \cdot \prod_{h=1}^{m_Y} (\alpha_{Y,h}^R)^{u_h} \quad (5)$$

$$r_j^S = k_S \cdot C_j^S \cdot \prod_{i=1}^{m_X} (\alpha_{X,i}^S)^{v_i} \cdot \prod_{h=1}^{m_Y} (\alpha_{Y,h}^S)^{u_h} \quad (6)$$

140 where r_j is the reaction rate for the j^{th} enantiomer-specific isotopologue of R or S enantiomer, α is
 141 the fractionation factor as defined in Eqs. 3 and 4, C_j is the concentration of the j^{th} enantiomer-
 142 specific isotopologue, and m , n , v and u are defined in Eqs. 1 and 2.

143 The concentration change of R and S enantiomers is described by tracking each enantiomer-specific
 144 isotopologue, respectively:

$$\frac{dC_j^R}{dt} = -r_j^R \quad (7)$$

$$\frac{dC_j^S}{dt} = -r_j^S \quad (8)$$

145

146 where C_j^R and C_j^S are the concentrations of the j^{th} R and S enantiomer-specific isotopologues, t is the
 147 time, and r_j is the reaction rate of the j^{th} enantiomer-specific isotopologue. The concentrations of
 148 individual enantiomers are obtained by summing the concentration of each enantiomer-specific
 149 isotopologue. The initial concentrations of the enantiomer-specific isotopologues are the product of
 150 the initial total concentration of R and S enantiomers with the corresponding initial abundances (Eqs.
 151 1 and 2).

152 The enantiomer ratio (*ER*) and the enantiomer fraction (*EF*) are normally used to describe
 153 enantiomer enrichment of chiral compounds (Harner et al., 2000; Jammer et al., 2014; Qiu et al.,
 154 2014). In the proposed framework, *ER* and *EF* can be computed considering the concentrations of
 155 enantiomer-specific isotopologues:

$$ER = \frac{C_S}{C_R} = \frac{\sum_{j=1}^N C_j^S}{\sum_{j=1}^N C_j^R} \quad (9)$$

$$EF_R = \frac{C_R}{C_R + C_S} = \frac{\sum_{j=1}^N C_j^R}{\sum_{j=1}^N C_j^R + \sum_{j=1}^N C_j^S} \quad (10)$$

$$EF_S = \frac{C_S}{C_R + C_S} = \frac{\sum_{j=1}^N C_j^S}{\sum_{j=1}^N C_j^R + \sum_{j=1}^N C_j^S} \quad (11)$$

156

157 where C_R and C_S are the concentrations of individual enantiomers, C_j is the concentration of each
 158 enantiomer-specific isotopologue for R or S enantiomer, and N is the total number of enantiomer-
 159 specific isotopologues.

160 The isotope ratios of elements X and Y at positions experiencing isotope effects in R or S
 161 enantiomer-specific isotopologues are calculated by considering the total number of heavy and light
 162 isotopes (Jin et al., 2011), and are expressed as:

$$R'_{X,R} = \frac{\text{Tot}(X_H)}{\text{Tot}(X_L)} = \frac{C_j^R \cdot \sum_{i=1}^{m_X} v_i}{C_j^R \cdot \sum_{i=1}^{m_X} (1-v_i)} \quad (12)$$

$$R'_{X,S} = \frac{\text{Tot}(X_H)}{\text{Tot}(X_L)} = \frac{C_j^S \cdot \sum_{i=1}^{m_X} v_i}{C_j^S \cdot \sum_{i=1}^{m_X} (1-v_i)} \quad (13)$$

$$R'_{Y,R} = \frac{\text{Tot}(Y_H)}{\text{Tot}(Y_L)} = \frac{C_j^R \cdot \sum_{h=1}^{m_Y} u_h}{C_j^R \cdot \sum_{h=1}^{m_Y} (1-u_h)} \quad (14)$$

$$R'_{Y,S} = \frac{\text{Tot}(Y_H)}{\text{Tot}(Y_L)} = \frac{C_j^S \cdot \sum_{h=1}^{m_Y} u_h}{C_j^S \cdot \sum_{h=1}^{m_Y} (1-u_h)} \quad (15)$$

163 in which R'_X and R'_Y are the isotope ratios of all the X and Y atoms on isotopically-sensitive
 164 positions of each enantiomer at a given point in time, C_j is the concentration of the j^{th} enantiomer-
 165 specific isotopologue at that point in time, and m , v and u are defined in Eqs. 1 and 2.

166 Enantiomer-specific isotope ratios (i.e., stable isotope ratios of individual enantiomers) are
 167 calculated at each point in time by taking into account changes of stable isotope ratios at
 168 fractionating positions and the dilution effects from non-fractionating positions in the enantiomer
 169 molecules as well as the initial bulk isotope ratio R_0 :

$$R_{X,R} = R'_{X,R} \cdot \frac{m_X}{n_X} + R_{0,X} \cdot \frac{n_X - m_X}{n_X} \quad (16)$$

$$R_{X,S} = R'_{X,S} \cdot \frac{m_X}{n_X} + R_{0,X} \cdot \frac{n_X - m_X}{n_X} \quad (17)$$

$$R_{Y,R} = R'_{Y,R} \cdot \frac{m_Y}{n_Y} + R_{0,Y} \cdot \frac{n_Y - m_Y}{n_Y} \quad (18)$$

170

$$R_{Y,S} = R'_{Y,S} \cdot \frac{m_Y}{n_Y} + R_{0,Y} \cdot \frac{n_Y - m_Y}{n_Y} \quad (19)$$

171 where R is the enantiomer-specific isotope ratio of element X or Y, R' is the corresponding isotope
 172 ratios of atoms at fractionating positions as computed in Eqs. 12-15.

173 Although a few recent contributions reported enantiomer-specific isotope ratios (ESIA), bulk
 174 isotope ratios determined by compound specific isotope analysis (CSIA) are commonly measured in
 175 most experimental studies. Bulk isotope ratios can be related to enantiomer-specific isotope ratios
 176 by the following weighted averages:

$$R_X = R_{X,R} \cdot EF_R + R_{X,S} \cdot EF_S \quad (20)$$

$$R_Y = R_{Y,R} \cdot EF_R + R_{Y,S} \cdot EF_S \quad (21)$$

177 where R_X and R_Y are the bulk isotope ratios of a chiral organic compound, $R_{X,R}$, $R_{X,S}$, $R_{Y,R}$ and $R_{Y,S}$ are
 178 the enantiomer-specific isotope ratios and EF_R and EF_S are the enantiomer fractions of individual
 179 enantiomers as defined in Eqs. 10 and 11.

180 The proposed model is developed in MATLAB® and it is applied to describe contaminant
 181 degradation in batch systems. The governing equations presented above (Eqs. 5-8) are solved for
 182 three selected illustrative examples of chiral compounds degradation. The specific derivation of the
 183 governing equations for the first illustrative example is described in the Supplementary Material.
 184 The document also provides a table summarizing the enantiomer-specific isotopologues and their
 185 number for the different examples considered. In all cases the reaction kinetics, described with a
 186 first-order or with a Michaelis-Menten formulation, were fitted to the concentration data provided in
 187 recently published experimental studies. The trust-region-reflective method implemented in the
 188 MATLAB® function *lsqnonlin* was used to minimize the sum of normalized squared errors
 189 between the observed and simulated concentration data. Enantiomer ratios and fractions, as well as

190 stable isotope ratios, were not fitted but evaluated with Eqs. 9-21 and directly compared to the
191 experimental results. Details on the fitting procedure, as well as an overview of the fitted
192 parameters are also available in the Supplementary Material.

193

194 **2.2. Examples of chiral pesticides degradation**

195 We test our modeling approach considering the degradation of three important chiral pesticides.
196 These examples are enzymatic degradation of dichlorprop (DCPP), enzymatic degradation of
197 mecoprop methyl ester (MCPPM) and aerobic and anaerobic biodegradation of α -
198 hexachlorocyclohexane (α -HCH). The chemical structures, the reaction mechanisms, the target
199 stable isotopes and the reactive bonds of these chiral compounds are illustrated in Table 1. Recent
200 experimental studies have provided high-quality data on enantioselectivity as well as on compound
201 specific (CSIA) and enantiomer specific stable isotope analysis (ESIA) for these chemicals and are
202 used to validate the joint quantitative approach proposed in this study.

203 Dichlorprop (DCPP) is a phenoxy acid commonly used as herbicide to control weeds. It is
204 frequently detected in groundwater systems (Spliid and Køppen, 1998). Enantiomer fractionation
205 and enantiomer specific carbon isotope fractionation have been observed during enzymatic
206 degradation of DCPP by enzyme RdpA from *Sphingobium herbicidovorans* MH (Qiu et al., 2014).
207 In order to investigate enantiomer-specific degradation mechanisms of DCPP, a two-dimensional
208 approach combining enantiomer analysis (EA) and enantiomer specific isotope analysis (ESIA) has
209 been applied. The data provided for DCPP degradation were used to validate the capability of the
210 proposed modeling approach to simultaneously predict the evolution of R- and S-DCPP enantiomer
211 concentrations, the formation of the reaction product, as well as the joint evaluation of C-ESIA
212 isotope ratios and enantiomer fractionation.

213 Mecoprop methyl ester (MCPPM) is a phenoxyalkanoic methyl herbicide, which is a contaminant
214 frequently found in aquatic environments. Enantiomer fractionation and compound specific isotope
215 fractionation (CSIA) of this chemical have been recently observed during enzymatic reactions by
216 different types of lipase enzymes from distinct microbial strains including *Pseudomonas*
217 *fluorescens*, *Candida rugose* and *Pseudomonas cepacia* (Jammer et al., 2014). This dataset was of
218 interest since it allowed testing the ability of the integrated model to characterize distinct reaction
219 pathways by combining enantiomer analysis (EA) and bulk (i.e., compound average) isotope ratios
220 from compound specific isotope analysis (CSIA).

221 The third and final application is focused on biodegradation of α -Hexachlorocyclohexane (α -HCH).
222 α -HCH is one of the dominant byproducts during the production of Lindane (γ -HCH), a widely
223 produced and applied insecticide (Lal et al., 2010; Phillips et al., 2005). Carbon ESIA and
224 enantiomer analysis (EA) have been applied to investigate biodegradation of α -HCH by different
225 microbial strains including *S. indicum* strain B90A, *S. japonicum* strain UT26 and *Clostridium*
226 *pasterianum* (Badea et al., 2011; Bashir et al., 2013). Biodegradation of α -HCH occurs under both
227 aerobic and anaerobic conditions, involving dehydrochlorination and dichloro-elimination,
228 respectively. We applied our model to reproduce the observed enantiomer and stable isotope signals
229 and to differentiate enantiomer-specific degradation pathways of α -HCH. Besides the
230 experimentally investigated combination of C-ESIA with EA (Bashir et al., 2013), the validated
231 model has been used to explore the potential of another combined two-dimensional approach (i.e.,
232 C-CSIA combined with EA) to characterize different isotope and enantiomer selective reaction
233 mechanisms.

234

235 **Table 1.** Chemical structures, enantiomers, stable isotopes and reaction mechanisms for the considered chiral
236 organic pesticides.

Compound	Chemical structure	Reaction (and Mechanism)	Isotope	Reactive bonds	Reference
Dichlorprop (DCPP)	<p>R-DCPP S-DCPP</p>	enzymatic reaction (oxidation of C-H bond)	$^{13}\text{C}/^{12}\text{C}$	C-H	Qiu et al., 2014
Mecoprop methyl ester (MCPMM)	<p>R-MCPPM S-MCPPM</p>	enzymatic reaction (hydrolysis)	$^{13}\text{C}/^{12}\text{C}$	C-O	Jammer et al., 2014
α -hexachlorocyclohexane (HCH)	<p>(+)-α-HCH (-)-α-HCH</p>	aerobic degradation (dehydrochlorination)	$^{13}\text{C}/^{12}\text{C}$	H-C-C-Cl	Badea et al., 2011 Bashir et al., 2013
		anaerobic degradation (dichloro-elimination)	$^{13}\text{C}/^{12}\text{C}$	Cl-C-C-Cl	

237

238

239

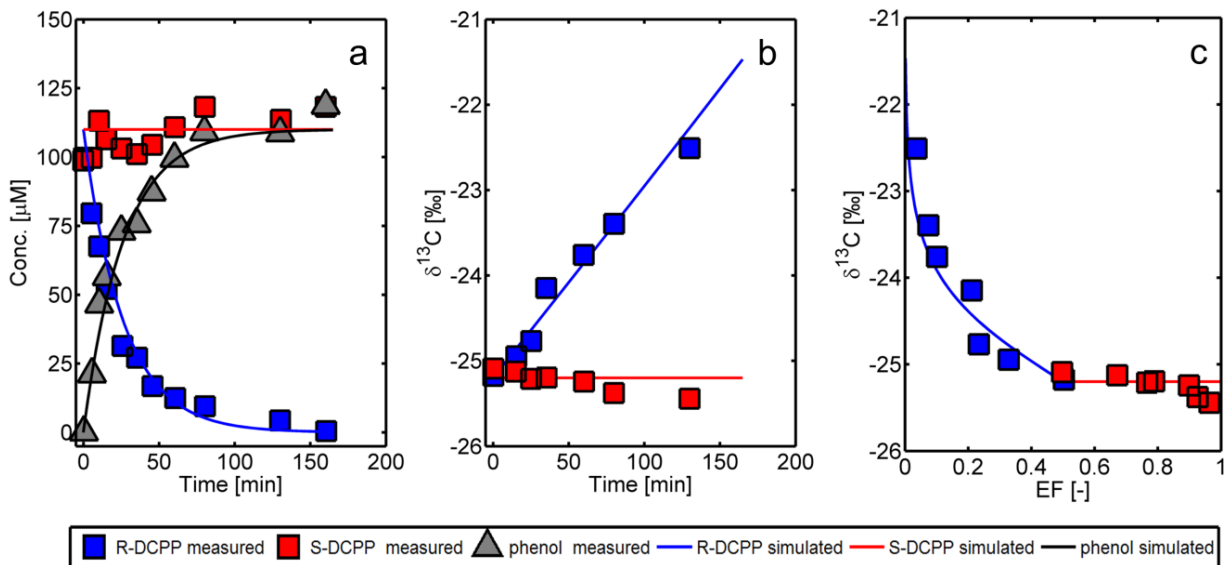
240

241 3. Results and discussion

242 3.1. Enzymatic degradation of dichlorprop (DCPP)

243 Experimental data on concentration evolution of DCPP and its main metabolite (phenol),
244 enantioselective effects and enantiomer specific carbon isotope fractionation were measured during
245 degradation of this pesticide by enzyme RdpA from *Sphingobium herbicidovorans* MH (Qiu et al.,
246 2014). The reported experimental observations are shown as symbols in Fig. 1 together with the
247 outcomes of the simulations using the proposed integrated approach (solid lines). The enantiomer
248 R-DCPP (blue) is consumed according to a first-order degradation kinetic with a reaction rate
249 constant $k_R=0.038\pm 0.003 \text{ min}^{-1}$, forming phenol (gray) as metabolite. The concentration of the other
250 isomer (S-DCPP), instead, remains constant due to the selectivity of the RdpA enzymes that
251 exclusively degrade the R enantiomer (Fig. 1a). The model accurately captures both the

252 consumption of the chiral pesticide degradation and the production of the metabolite. Also the
253 isotopic signals observed during enzymatic degradation of DCPD are considerably different
254 between R and S enantiomers. In fact, significant carbon isotope fractionation occurs only for R-
255 DCPD, varying from -25.1 ‰ to -22.5 ‰, whereas no significant carbon isotope fractionation
256 occurs for S-DCPD. Fig. 1b illustrates the observed and simulated temporal trends of carbon isotope
257 ratios for both DCPD enantiomers. The model reproduces satisfactorily the linear increase of $\delta^{13}\text{C}$
258 observed for R-DCPD as well as the stable isotopic composition of S-DCPD. Illustrative plots are
259 also obtained by representing the stable carbon isotope signature as a function of the enantiomer
260 fraction (Fig. 1c). The fast consumption of R-DCPD leads to decreasing R-enantiomer fraction
261 (from 50% to 4%) and increasing S-enantiomer fraction (50% to 96%). Interestingly, a nonlinear
262 relationship is observed for R-DCPD due to the considerably larger extent of enantiomer
263 fractionation compared to the relatively small carbon isotope fractionation. This behavior is
264 accurately predicted by the model, which results in a concave upward profile with increasing
265 steepness as the reaction proceeds and the fraction of R-DCPD progressively decreases. The
266 quantitative interpretation of the experimental data with the proposed integrated modeling approach
267 allows simultaneously and accurately capturing the concentrations, stable isotopes and
268 enantioselective behavior observed in the experimental study. A specific advantage that is worth
269 noticing is the good performance of the model when its outcomes are compared to the experimental
270 data in the two-dimensional plot combining stable isotopes and enantiomer fractionation.



271

272 **Figure 1.** Isotope and enantiomer fractionation during enzymatic degradation of dichlorprop (DCPP). The
 273 symbols represent experimental data reported by Qiu et al., 2014 and the solid lines are simulation results: (a)
 274 concentration change of R- (blue squares) and S- (red squares) enantiomers of DCPP; (b) carbon isotope
 275 fractionation for both R- and S-DCPP; and (c) two-dimensional plot combining carbon isotope and
 276 enantiomer fractionation.

277

278

279

3.2. Enzymatic hydrolysis of mecoprop methyl ester (MCPPM)

280

281

282

283

284

285

286

287

288

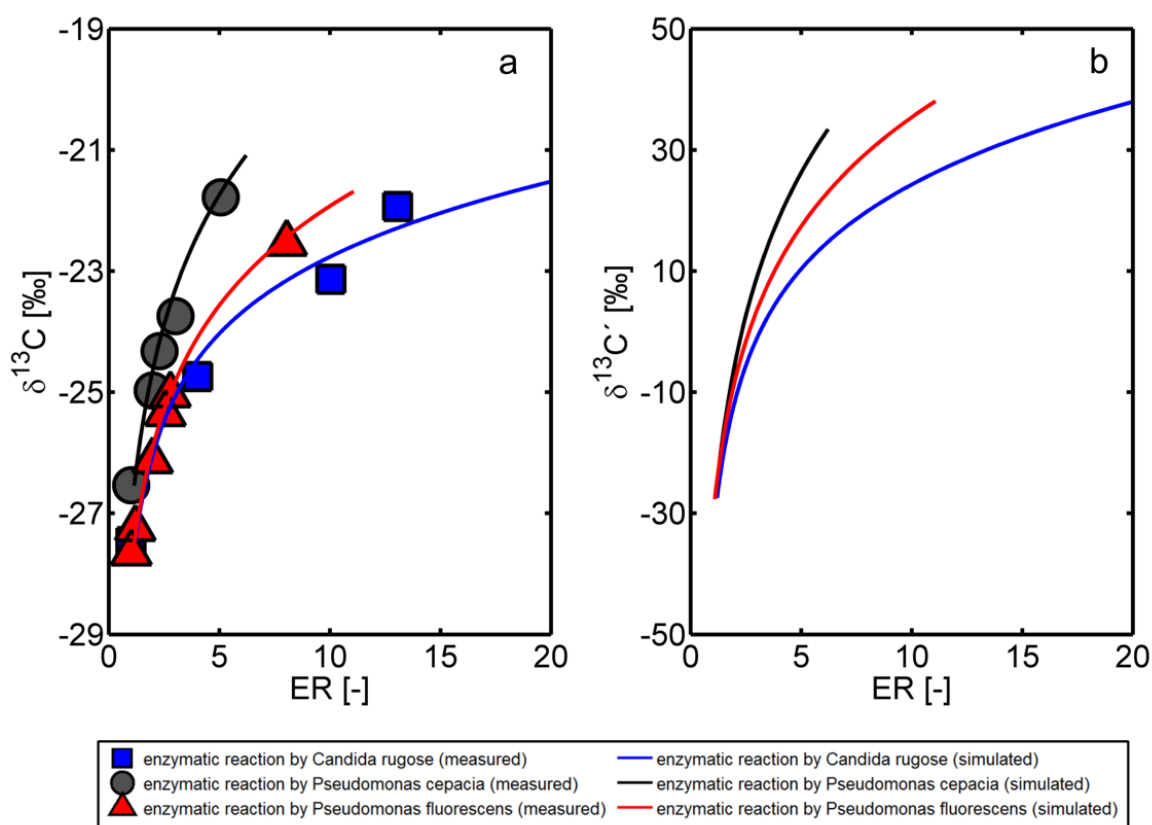
289

290

Enantiomer and carbon isotope fractionation have been observed during enzymatic hydrolysis of a phenoxyalkanoic methyl herbicide, mecoprop methyl ester (MCPPM) (Jammer et al., 2014). The enzymatic reactions by different types of lipase enzymes, *Pseudomonas fluorescens*, *Candida rugose* and *Pseudomonas cepacia* were investigated combining compound specific stable isotope analysis (C-CSIA) with enantiomer analysis (EA). We simulate MCPPM degradation with a first-order kinetic model according to the unified framework outlined in Section 2 to integrate the quantitative description of enantioselectivity and stable isotope fractionation. The governing equations for the S and R enantiomers of MCPPM and the concentration evolution in the experiments conducted with the enzymes of the three different strains are reported in the Supplementary Material. Two-dimensional plots combining stable isotope and enantiomer fractionation are shown in Fig. 2. Notice that enantiomer fractionation is expressed as enantiomer

291 ratio, *ER*, since CSIA data do not allow discriminating between the different enantiomers and, thus,
292 can only be presented as a function of *ER* rather than of the enantiomer fraction, *EF*. The carbon
293 isotope fractionation of MCPPM occurs at similar extents for the three enzymatic reactions, where
294 the following shifts in $\delta^{13}\text{C}$ values were observed: 4.7 ‰ for *Pseudomonas cepacia*, 5.2 ‰ for
295 *Pseudomonas fluorescens* and 5.6 ‰ for *Candida rugose*. Therefore, in this case, C-CSIA alone is
296 not conclusive to clearly identify the three different enzymatic reactions. To this end, a two-
297 dimensional approach combining C-CSIA with enantiomer analysis is highly beneficial and was
298 proposed in the experimental study (Jammer et al., 2014). In fact, distinct enantiomer enrichments
299 are observed for the three investigated reactions. Combining enantiomer fractionation and C-CSIA
300 signals allows distinguishing and clearly visualizing the three enzymatic reactions (Fig. 2a).
301 Similarly to what has been observed for DCPD degradation, nonlinear relationships between
302 compound specific carbon isotope ratios and enantiomeric ratios are also observed during
303 enzymatic reactions of MCPPM. This is due to the much more significant changes of enantiomer
304 ratios that are three orders of magnitude larger than the shifts in stable isotope ratios. The nonlinear
305 behavior is well captured by the outcomes of the model that accurately reproduce the different
306 trends observed for the three enzymatic reactions. The model results show bending trends that are
307 more pronounced for the enzymatic reactions by *Candida rugose* and *Pseudomonas fluorescens*,
308 which are characterized by more extensive enantiomer fractionation. The profiles characterizing the
309 reaction mechanisms progressively become less steep at later reaction times and show extents of
310 slope variations of 85% for *Pseudomonas cepacia*, 93% for *Pseudomonas fluorescens* and for 98%
311 for *Candida rugose*. An additional direct outcome of the proposed modeling approach is the
312 quantification of isotope ratios directly at the position experiencing isotope effects. This naturally
313 stems from the model formulation based on enantiomer-specific isotopologues and its capability to
314 track isotope ratios at isotopically sensitive positions (Eqs. 12-15). Position-specific isotope data

315 were not available for MCPPM degradation, but recent advances have shown the capability of
 316 measuring changes of isotope ratios at specific molecular positions of certain organic compounds
 317 (e.g., Wuerfel et al., 2013) and we expect that a number of future investigations will provide such
 318 data for a wide range of organic pollutants. In Fig. 2b we present modeling results to describe
 319 position-specific isotope fractionation occurring at the reactive carbon atom during enzymatic
 320 hydrolysis of MCPPM combined with the corresponding enantiomer ratios. The three distinct
 321 reactions are clearly identified in the two-dimensional plot with the advantage that the carbon
 322 isotope fractionation reported in the ordinate axis is now characterized by a larger magnitude (i.e.,
 323 60 ‰ for *Pseudomonas cepacia*, 66 ‰ for *Pseudomonas fluorescens* and 75 ‰ for *Candida*
 324 *rugose*), since the model directly predicts the fractionation at reactive position without the dilution
 325 effects of other non-reactive carbon atoms present in the pesticide molecule.



326

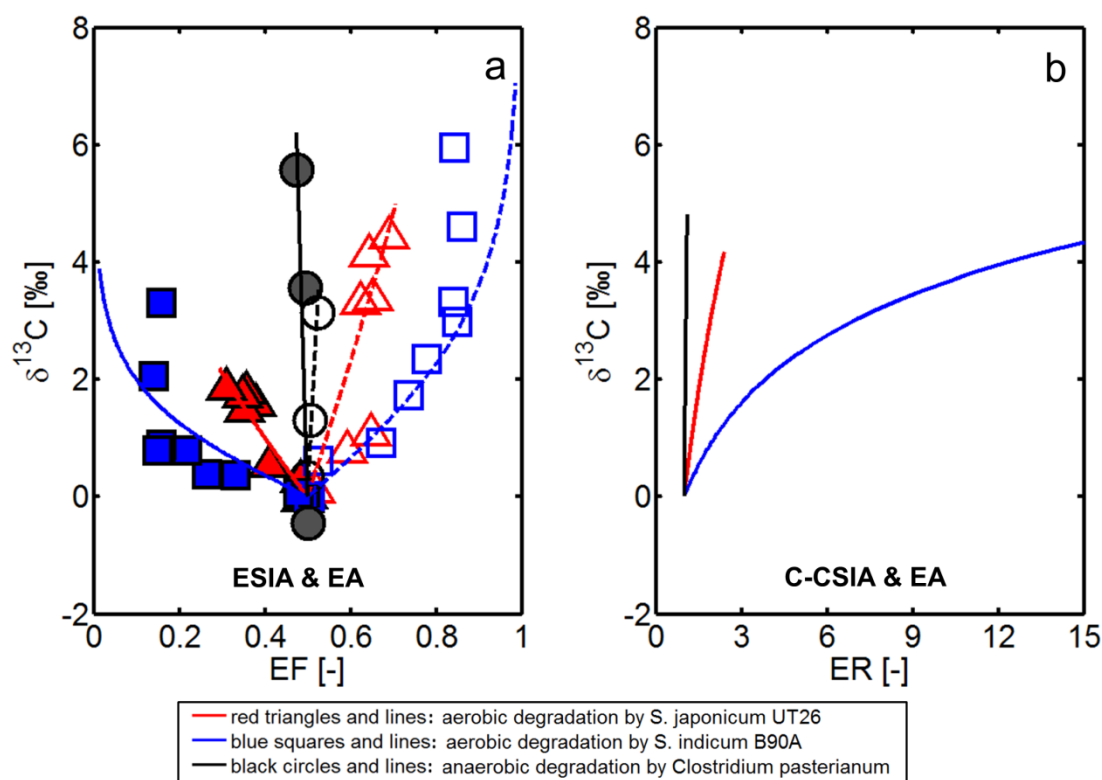
327 **Figure 2.** Isotope and enantiomer fractionation during enzymatic degradation of mecoprop methyl ester
 328 (MCPPM): (a) observed (symbols, Jammer et al., 2014) and simulated (lines) bulk isotope ratios and
 329 enantiomer ratios; (b) simulated position-specific isotope fractionation as function of the enantiomer ratio.

330

331 **3.3. Aerobic and anaerobic biodegradation of α -hexachlorocyclohexane (α -HCH)**

332 As last illustrative example to validate the proposed approach, we consider biodegradation of
333 hexachlorocyclohexane which has been experimentally studied combining enantiomer analysis and
334 enantiomer-specific isotope analysis, ESIA (Badea et al., 2011; Bashir et al., 2013). The
335 degradation of α -HCH by different microbial strains including *S. indicum* strain B90A, *S.*
336 *japonicum* strain UT26 and *Clostridium pasterianum* was investigated in batch culture experiments.
337 We provide a quantitative, model-based interpretation of the experimental data reported in the study
338 of Bashir et al. 2013. We describe the observed concentration trends during α -HCH biodegradation
339 with Michaelis-Menten kinetics coupled to the dynamics of growth and decay of the different
340 microbial strains (Supplementary Material). The modeling framework outlined above was adopted
341 to jointly describe the evolution of the two α -HCH enantiomers (identified by their optical activity:
342 + and -) and the enantiomer-specific carbon isotope fractionation. As shown in Fig. 3a, the reactions
343 by different microbial strains are clearly identified in the two-dimensional plot. Aerobic degradation
344 by *S. indicum* strain B90A (squares) and *S. japonicum* strain UT26 (triangles) as well as the
345 anaerobic biodegradation by *Clostridium pasterianum* (circles) yield different extents of both
346 enantiomer and enantiomer specific carbon isotope fractionation. Anaerobic biodegradation of α -
347 HCH resulted in significant carbon isotope fractionation (by 6.0 ‰ and 3.2 ‰ for (+) and (-) α -
348 HCH, respectively), but almost no enantiomer fractionation was observed comparing with the
349 aerobic reactions. This indicates that the enzymes involved in the anaerobic degradation of α -HCH
350 are rather isotopically-sensitive than enantiomer selective. Although the aerobic biodegradation by
351 the two different strains have the same reaction mechanisms involving dehydrochlorination (Table
352 1), different extents of enantiomer fractionation were observed. The enantiomer fraction of α -HCH
353 varies by 17 % and 34 % for aerobic degradation with strain UT26 (triangles) and strain B90A

354 (squares), respectively. The distinction in the enantiomer fractionation might be caused by the
 355 differences in the enzyme selectivity for the (+) and (-) enantiomers between the two microbial
 356 strains. This observation for α -HCH degradation (Bashir et al., 2013) is also consistent with
 357 previous findings on enantiomer fractionation of other chiral compounds (e.g., Zipper et al., 1998).
 358 The outcomes of the proposed modeling approach successfully reproduce the enantiomer-specific
 359 isotope fractionation and the enantiomer enrichments observed in the experiments. The model
 360 captures the distinct patterns observed during α -HCH degradation by the three different microbial
 361 strains under both aerobic and anaerobic conditions.



362

363 **Figure 3.** Isotope and enantiomer fractionation during aerobic and anaerobic biodegradation of α -
 364 hexachlorocyclohexane (α -HCH) by three different microbial strains. The markers (closed symbols for (+) α -
 365 HCH and open symbols for (-) α -HCH) represent the experimental data reported in Bashir et al., 2013 and
 366 Badea et al., 2011 and the solid lines are the simulation results (a). The bulk carbon isotope ratios are plotted
 367 with the enantiomer ratios in panel (b).

368

369 The modeling approach, validated above with the data combining enantiomer specific isotope
370 analysis (C-ESIA) with enantiomer analysis (EA), was also used to test other possible combinations
371 of two-dimensional approaches to identify and assess isotope and enantiomer selective reaction
372 mechanisms. To this end, we consider the biodegradation of α -HCH by the three microbial strains
373 investigated by Badea et al. (2011) and Bashir et al. (2013) as well as the same Michaelis-Menten
374 kinetics described above, and we explore the potential of a different combination of stable isotope
375 and enantiomer analyses.

376 We consider a scenario analogous to the experimentally investigated case of α -HCH degradation
377 discussed above but with the only difference that bulk (and not enantiomer specific) carbon isotope
378 analysis is combined with enantiomer analysis. The results are reported in the two-dimensional plot
379 shown in Fig. 3b. The changes in carbon isotope ratios are reported on the ordinate axis whereas the
380 enantiomer ratios (*ER*) are reported on the abscissa. The three different reactions are still adequately
381 identified. The profile of aerobic degradation of *S. indicum* strain B90A (blue line) is clearly
382 distinguished due to the strong enantiomer fractionation compared to the other two cases. The
383 results characterizing α -HCH degradation by *S. japonicum* strain UT26 (red line) and *Clostridium*
384 *pasterianum* (black line) are still separated but appear to be closer than in the case of C-ESIA (Fig.
385 3a). The difference observed between the scenario combining C-CSIA with EA (Figure 3b) and the
386 experimentally investigated case of C-ESIA (Figure 3a) stems from the fact that CSIA cannot
387 determine isotope ratios of individual enantiomers, but only the bulk carbon isotope ratios of the
388 mixture of the two α -HCH enantiomers. Notice that the x-axis in Figure 3b is different from the one
389 in Figure 3a. In fact, without ESIA isotope data the carbon isotope ratios from CSIA can only be
390 reported as a function of the enantiomer ratio and not as a function of enantiomer fraction.

391 The model-based analysis has shown that a combined interpretation of stable isotope and
392 enantiomer fractionation is required when enantiomer-specific mechanisms play a crucial role

393 during chiral pesticides transformations. As shown in Fig. 3a and 3b, the combination of carbon
394 isotope analysis (C-ESIA or C-CSIA) with enantiomer analysis can unambiguously distinguish the
395 three reaction pathways of α -HCH degradation.

396

397 **4. Conclusions**

398 Multiple lines of evidence are required to understand the environmental fate and to decipher
399 intricate transformation processes of chiral pesticides in natural and engineered aquatic systems. To
400 this end, advances in analytical capabilities have allowed to accompany traditional determination of
401 pollutants and metabolites aqueous concentrations with measurements of enantiomer and multi-
402 element stable isotope fractionation. In particular, the combination of enantioselective
403 measurements and compound specific isotope analysis has recently emerged as a powerful tool to
404 characterize biotransformation reactions. Different reaction mechanisms of chiral pesticides are
405 effectively identified in two-dimensional plots combining enantiomer fractionation with stable
406 isotope ratios. The approach proposed in this study provides a unified, quantitative tool for
407 interpretation of chiral pesticides degradation based on the evolution of enantiomer-specific
408 isotopologues. The model has been validated with data from experimental studies on enzymatic
409 degradation of dichlorprop (DCPP), enzymatic degradation of mecoprop methyl ester (MCPPM)
410 and microbial degradation of α -hexachlorocyclohexane (α -HCH) by different bacterial strains. A
411 good agreement between the outcomes of the numerical simulations and the experimental data was
412 obtained for all the different compounds and degradation pathways. The normalized root mean
413 squared error (NRMSE) was used as a measure of the goodness of fit and yielded values in a range
414 0.021-0.355. Detailed values of NRMSE for the different concentrations, stable isotopes and
415 enantiomers datasets are reported in the Supplementary Material (Table S5).

416 The main features of the proposed approach can be summarized in the following points:

- 417 - First-principle based and self-consistent integration of concentrations, stable isotopes and
418 enantiomers data. The simultaneous description and the joint interpretation of these
419 quantities allow naturally capturing the nonlinearity stemming from the significantly
420 different extents of enantiomer and stable isotope fractionation. This can help overcoming
421 difficulties that may arise in applying linear Rayleigh-based evaluations in presence of
422 strong fractionating effects, as well as linear regressions in two-dimensional plots of stable
423 isotopes vs. enantiomers fractionation.
- 424 - By tracking enantiomer-specific isotopologues the model is capable to identify and
425 characterize isotope and enantiomer selective reaction mechanisms. The former involves
426 shifts in isotopic compositions due to the cleavage of chemical bonds, whereas the latter
427 results from the differential interactions of individual chiral pesticides' enantiomers with
428 microbial enzymatic systems. The model formulation incorporates the mechanistic
429 description of both fractionating systems.
- 430 - As illustrated for the case of α -HCH biodegradation, the model can help assessing the
431 potential, the advantages as well as the limitations of different two-dimensional approaches
432 combining enantiomer analysis (EA) with isotope analysis (CSIA and ESIA).

433 In this study, specific examples of chiral pesticides degradation have been selected to illustrate the
434 features of the proposed unified model. The modeling approach was applied to quantitatively
435 describe the integrated evolution of carbon isotope and enantiomer ratios for various chiral organic
436 pollutants. However, as illustrated in the mathematical formulation, the proposed model provides a
437 general framework that allows combining enantiomer fractionation with the description of multi-
438 element isotope fractionation. Furthermore, besides applications in batch aqueous solutions, the
439 model can be further developed to describe contaminant degradation in more complex
440 environmental systems including transport processes and interphase mass transfer.

441

442

443 **Acknowledgements**

444 The authors would like to acknowledge the support of the Deutsche Forschungsgemeinschaft (Grant
445 RO4169/2-1) and the internal funding from the Department of Environmental Engineering at the
446 Technical University of Denmark. Constructive comments of three anonymous reviewers helped
447 improving the quality of the manuscript.

448

449 **Appendix A. Supplementary Material**

450 Supplementary material related to this article includes the model formulation and implementation,
451 as well as the fitting procedure used to validate the proposed modeling approach with the
452 experimental datasets.

453 **Reference**

- 454 Badea, S.L., Vogt, C., Gehre, M., Fischer, A., Danet, A.F., Richnow, H.H., 2011. Development of an
455 enantiomer-specific stable carbon isotope analysis (ESIA) method for assessing the fate of ??-
456 hexachlorocyclo-hexane in the environment. *Rapid Commun. Mass Spectrom.* 25, 1363–1372.
457 doi:10.1002/rcm.4987
- 458 Bashir, S., Fischer, A., Nijenhuis, I., Richnow, H.H., 2013. Enantioselective carbon stable isotope
459 fractionation of hexachlorocyclohexane during aerobic biodegradation by *Sphingobium* spp. *Environ.*
460 *Sci. Technol.* 47, 11432–11439. doi:10.1021/es402197s
- 461 Bashir, S., Hitzfeld, K.L., Gehre, M., Richnow, H.H., Fischer, A., 2015. Evaluating degradation of
462 hexachlorocyclohexane (HCH) isomers within a contaminated aquifer using compound-specific stable
463 carbon isotope analysis (CSIA). *Water Res.* 71, 187–196. doi:10.1016/j.watres.2014.12.033
- 464 Bollmann, U.E., Tang, C., Eriksson, E., Jönsson, K., Vollertsen, J., Bester, K., 2014. Biocides in urban
465 wastewater treatment plant influent at dry and wet weather: Concentrations, mass flows and possible
466 sources. *Water Res.* 60, 64–74. doi:10.1016/j.watres.2014.04.014
- 467 Breider, F., Hunkeler, D., 2011. Position-specific carbon isotope analysis of trichloroacetic acid by gas
468 chromatography/isotope ratio mass spectrometry. *Rapid Commun. Mass Spectrom.* 25, 3659–3665.
469 doi:10.1002/rcm.5276
- 470 Eckert, D., Rolle, M., Cirpka, O. a., 2012. Numerical simulation of isotope fractionation in steady-state
471 bioreactive transport controlled by transverse mixing. *J. Contam. Hydrol.* 140-141, 95–106.
472 doi:10.1016/j.jconhyd.2012.08.010
- 473 Elsayed, O.F., Maillard, E., Vuilleumier, S., Nijenhuis, I., Richnow, H.H., Imfeld, G., 2014. Using
474 compound-specific isotope analysis to assess the degradation of chloroacetanilide herbicides in lab-
475 scale wetlands. *Chemosphere* 99, 89–95. doi:10.1016/j.chemosphere.2013.10.027
- 476 Elsner, M., Zwank, L., Hunkeler, D., Schwarzenbach, R.P., 2005. A new concept linking observable stable
477 isotope fractionation to transformation pathways of organic pollutants. *Environ. Sci. Technol.* 39,
478 6896–6916. doi:10.1021/es0504587
- 479 Fenner, K., Canonica, S., Wackett, L.P., Elsner, M., 2013. Evaluating pesticide degradation in the
480 environment: blind spots and emerging opportunities. *Science* 341, 752–8.
481 doi:10.1126/science.1236281
- 482 Grzybkowska, A., Kaminski, R., Dybala-Defratyka, A., 2014. Theoretical predictions of isotope effects
483 versus their experimental values for an example of uncatalyzed hydrolysis of atrazine. *Phys. Chem.*
484 *Chem. Phys.* 16, 15164. doi:10.1039/c4cp00914b
- 485 Harner, T., Wiberg, K., Norstrom, R., 2000. Enantiomer fractions are preferred to enantiomer ratios for
486 describing chiral signatures in environmental analysis. *Environ. Sci. Technol.* 34, 218–220.
487 doi:10.1021/es9906958
- 488 Hofstetter, T.B., Reddy, C.M., Heraty, L.J., Berg, M., Sturchio, N.C., 2007. Carbon and chlorine isotope
489 effects during abiotic reductive dechlorination of polychlorinated ethanes. *Environ. Sci. Technol.* 41,
490 4662–4668. doi:10.1021/es0704028
- 491 Jammer, S., Voloshenko, A., Gelman, F., Lev, O., 2014. Chiral and isotope analyses for assessing the
492 degradation of organic contaminants in the environment: Rayleigh dependence. *Environ. Sci. Technol.*
493 48, 3310–8. doi:10.1021/es4039209
- 494 Jin, B., Haderlein, S.B., Rolle, M., 2013. Integrated carbon and chlorine isotope modeling: Applications to
495 chlorinated aliphatic hydrocarbons dechlorination. *Environ. Sci. Technol.* 47, 1443–1451.
496 doi:10.1021/es304053h
- 497 Jin, B., Laskov, C., Rolle, M., Haderlein, S.B., 2011. Chlorine Isotope Analysis of Organic Contaminants

- 498 Using GC–qMS: Method Optimization and Comparison of Different Evaluation Schemes. *Environ. Sci.*
499 *Technol.* 45, 5279–5286. doi:10.1021/es200749d
- 500 Jin, B., Rolle, M., 2014. Mechanistic approach to multi-element isotope modeling of organic contaminant
501 degradation. *Chemosphere* 95, 131–139. doi:10.1016/j.chemosphere.2013.08.050
- 502 Jin, B., Rolle, M., 2016. Position-specific isotope modeling of organic micropollutants transformation
503 through different reaction pathways. *Environ. Pollut.* 210, 94–103. doi:10.1016/j.envpol.2015.11.014
- 504 Jin, B., Rolle, M., Li, T., Haderlein, S.B., 2014. Diffusive fractionation of BTEX and chlorinated ethenes in
505 aqueous solution: Quantification of spatial isotope gradients. *Environ. Sci. Technol.* 48, 6141–6150.
506 doi:10.1021/es4046956
- 507 Lal, R., Pandey, G., Sharma, P., Kumari, K., Malhotra, S., Pandey, R., Raina, V., Kohler, H.-P.E., Holliger,
508 C., Jackson, C., Oakeshott, J.G., 2010. Biochemistry of microbial degradation of
509 hexachlorocyclohexane and prospects for bioremediation. *Microbiol. Mol. Biol. Rev.* 74, 58–80.
510 doi:10.1128/MMBR.00029-09
- 511 Lapworth, D.J., Baran, N., Stuart, M.E., Ward, R.S., 2012. Emerging organic contaminants in groundwater:
512 A review of sources, fate and occurrence. *Environ. Pollut.* 163, 287–303.
513 doi:10.1016/j.envpol.2011.12.034
- 514 Maier, M.P., Qiu, S., Elsner, M., 2013. Enantioselective stable isotope analysis (ESIA) of polar herbicides.
515 *Anal. Bioanal. Chem.* 405, 2825–2831. doi:10.1007/s00216-013-6745-0
- 516 McKnight, U.S., Rasmussen, J.J., Kronvang, B., Binning, P.J., Bjerg, P.L., 2015. Sources, occurrence and
517 predicted aquatic impact of legacy and contemporary pesticides in streams. *Environ. Pollut.* 200, 64–76.
518 doi:10.1016/j.envpol.2015.02.015
- 519 Milosevic, N., Qiu, S., Elsner, M., Einsiedl, F., Maier, M.P., Bensch, H.K. V, Albrechtsen, H.J., Bjerg, P.L.,
520 2013. Combined isotope and enantiomer analysis to assess the fate of phenoxy acids in a heterogeneous
521 geologic setting at an old landfill. *Water Res.* 47, 637–649. doi:10.1016/j.watres.2012.10.029
- 522 Pal, A., Gin, K.Y.H., Lin, A.Y.C., Reinhard, M., 2010. Impacts of emerging organic contaminants on
523 freshwater resources: Review of recent occurrences, sources, fate and effects. *Sci. Total Environ.* 408,
524 6062–6069. doi:10.1016/j.scitotenv.2010.09.026
- 525 Petrie, B., Barden, R., Kasprzyk-Hordern, B., 2014. A review on emerging contaminants in wastewaters and
526 the environment: Current knowledge, understudied areas and recommendations for future monitoring.
527 *Water Res.* 72, 3–27. doi:10.1016/j.watres.2014.08.053
- 528 Phillips, T.M., Seech, A.G., Lee, H., Trevors, J.T., 2005. Biodegradation of hexachlorocyclohexane (HCH)
529 by microorganisms. *Biodegradation* 16, 363–392. doi:10.1007/s10532-004-2413-6
- 530 Qiu, S., Gözdereliler, E., Weyrauch, P., Lopez, E.C.M., Kohler, H.P.E., Sørensen, S.R., Meckenstock, R.U.,
531 Elsner, M., 2014. Small ¹³C/¹²C fractionation contrasts with large enantiomer fractionation in aerobic
532 biodegradation of phenoxy acids. *Environ. Sci. Technol.* 48, 5501–5511. doi:10.1021/es405103g
- 533 Rügge, K., Juhler, R.K., Broholm, M.M., Bjerg, P.L., 2002. Degradation of the (R)- and (S)-enantiomers of
534 the herbicides MCPP and dichlorprop in a continuous field-injection experiment. *Water Res.* 36, 4160–
535 4164. doi:10.1016/S0043-1354(02)00131-8
- 536 Sakaguchi-Söder, K., Jager, J., Grund, H., Matthäus, F., Schüth, C., 2007. Monitoring and evaluation of
537 dechlorination processes using compound-specific chlorine isotope analysis. *Rapid Commun. Mass*
538 *Spectrom.* 21, 3077–3084. doi:10.1002/rcm.3170
- 539 Schmidt, T.C., Jochmann, M. a., 2012. Origin and Fate of Organic Compounds in Water: Characterization by
540 Compound-Specific Stable Isotope Analysis. *Annu. Rev. Anal. Chem.* 5, 133–155.
541 doi:10.1146/annurev-anchem-062011-143143
- 542 Schwarzenbach, R.P., Egli, T., Hofstetter, T.B., von Gunten, U., Wehrli, B., 2010. Global Water Pollution
543 and Human Health. *Annu. Rev. Environ. Resour.* doi:10.1146/annurev-environ-100809-125342

544 Schwarzenbach, R.P., Escher, B.I., Fenner, K., Hofstetter, T.B., Johnson, C.A., von Gunten, U., Wehrli, B.,
545 2006. The challenge of micropollutants in aquatic systems. *Science* 313, 1072–1077.
546 doi:10.1126/science.1127291

547 Spliid, N.H., Køppen, B., 1998. Occurrence of pesticides in Danish shallow ground water. *Chemosphere* 37,
548 1307–1316. doi:10.1016/S0045-6535(98)00128-3

549 Stenzel, A., Goss, K.U., Endo, S., 2013. Experimental determination of polyparameter linear free energy
550 relationship (pp-LFER) substance descriptors for pesticides and other contaminants: New
551 measurements and recommendations. *Environ. Sci. Technol.* 47, 14204–14214. doi:10.1021/es404150e

552 Świderek, K., Paneth, P., 2012. Extending limits of chlorine kinetic isotope effects. *J. Org. Chem.* 77, 5120–
553 5124. doi:10.1021/jo300682f

554 Thorling, L., 2015. Grundvand Status og udvikling 1989-2013, GEUS Report.
555 doi:10.1177/0961203307085124

556 Turner, J., Albrechtsen, H.J., Bonell, M., Duguet, J.P., Harris, B., Meckenstock, R., McGuire, K., Moussa, R.,
557 Peters, N., Richnow, H.H., Sherwood-Lollar, B., Uhlenbrook, S., van Lanen, H., 2006. Future trends in
558 transport and fate of diffuse contaminants in catchments, with special emphasis on stable isotope
559 applications. *Hydrol. Process.* 20, 205–213. doi:10.1002/hyp.6074

560 Van Breukelen, B.M., Rolle, M., 2012. Transverse hydrodynamic dispersion effects on isotope signals in
561 groundwater chlorinated solvents plumes. *Environ. Sci. Technol.* 46, 7700–7708.
562 doi:10.1021/es301058z

563 Vorkamp, K., Bossi, R., Bester, K., Bollmann, U.E., Boutrup, S., 2014. New priority substances of the
564 European Water Framework Directive: Biocides, pesticides and brominated flame retardants in the
565 aquatic environment of Denmark. *Sci. Total Environ.* 470-471, 459–468.
566 doi:10.1016/j.scitotenv.2013.09.096

567 Wong, C.S., 2006. Environmental fate processes and biochemical transformations of chiral emerging organic
568 pollutants. *Anal. Bioanal. Chem.* 386, 544–558. doi:10.1007/s00216-006-0424-3

569 Wuerfel, O., Greule, M., Keppler, F., Jochmann, M. a., Schmidt, T.C., 2013. Position-specific isotope
570 analysis of the methyl group carbon in methylcobalamin for the investigation of biomethylation
571 processes. *Anal. Bioanal. Chem.* 405, 2833–2841. doi:10.1007/s00216-012-6635-x

572 Zipper, C., Suter, M.J.F., Haderlein, S.B., Gruhl, M., Kohler, H.P.E., 1998. Changes in the enantiomeric
573 ratio of (R)- to (S)-mecoprop indicate in situ biodegradation of this chiral herbicide in a polluted
574 aquifer. *Environ. Sci. Technol.* 32, 2070–2076. doi:10.1021/es970880q

575

576